

PAPER

# Effect of pressure on the self-hole-doped superconductor $\text{RbGd}_2\text{Fe}_4\text{As}_4\text{O}_2$

To cite this article: J P Sun *et al* 2019 *J. Phys.: Condens. Matter* **31** 044001

View the [article online](#) for updates and enhancements.



**IOP | ebooks™**

Bringing you innovative digital publishing with leading voices to create your essential collection of books in STEM research.

Start exploring the collection - download the first chapter of every title for free.

# Effect of pressure on the self-hole-doped superconductor $\text{RbGd}_2\text{Fe}_4\text{As}_4\text{O}_2$

J P Sun<sup>1,6</sup>, Z-C Wang<sup>2</sup>, Z Y Liu<sup>1,3</sup>, S X Xu<sup>1,6</sup>, T Eto<sup>4</sup>, Y Sui<sup>3</sup>, B S Wang<sup>1,6,7</sup>,  
Y Uwatoko<sup>5</sup>, G-H Cao<sup>2</sup> and J-G Cheng<sup>1,6,7</sup> 

<sup>1</sup> Beijing National Laboratory for Condensed Matter Physics and Institute of Physics, Chinese Academy of Sciences, Beijing 100190, People's Republic of China

<sup>2</sup> Department of Physics, Zhejiang University, Hangzhou 310027, People's Republic of China

<sup>3</sup> Department of Physics, Harbin Institute of Technology, Harbin 150001, People's Republic of China

<sup>4</sup> Faculty of Engineering, Kurume Institute of Technology, Kurume, Fukuoka 830-0052, Japan

<sup>5</sup> Institute for Solid State Physics, University of Tokyo, Kashiwa, Chiba 277-8581, Japan

<sup>6</sup> School of Physical Sciences, University of Chinese Academy of Sciences, Beijing 100190, People's Republic of China

<sup>7</sup> Songshan Lake Materials Laboratory, Dongguan, Guangdong 523808, People's Republic of China

E-mail: [jgcheng@iphy.ac.cn](mailto:jgcheng@iphy.ac.cn)

Received 30 July 2018, revised 3 November 2018

Accepted for publication 14 November 2018

Published 13 December 2018



CrossMark

## Abstract

$\text{RbGd}_2\text{Fe}_4\text{As}_4\text{O}_2$  is a newly discovered self-hole-doped stoichiometric superconductor, which has a hybrid structure with separated double FeAs layers and exhibits a high superconducting transition temperature  $T_c = 35$  K. Here, we report the effect of pressure ( $P$ ) on its  $T_c$  and normal-state transport properties by measuring the temperature dependence of resistivity  $\rho(T)$  under various pressures up to 14 GPa with a cubic anvil cell apparatus. We found that the  $T_c$  is suppressed monotonically to ca. 12.5 K upon increasing pressure to 14 GPa with a slope change of  $T_c(P)$  at around 4 GPa. In addition, the low-temperature normal-state  $\rho(T)$ , which is proportional to  $T^n$ , also evolves gradually from a non-Fermi-liquid with  $n = 1$  at ambient pressure to a Fermi liquid with  $n = 2$  at  $P \geq 4$  GPa. Accompanying with the non-Fermi-liquid to Fermi-liquid crossover, the quadratic temperature coefficient of resistivity, which reflects the effective mass of charge carriers, also experiences a significant reduction as commonly observed in the vicinity of a magnetic quantum critical point (QCP). Our results indicate that the stoichiometric  $\text{RbGd}_2\text{Fe}_4\text{As}_4\text{O}_2$  at ambient pressure might be located near a QCP such that the enhanced critical spin fluctuations lead to high- $T_c$  superconductivity. The application of pressure should broaden the electronic bandwidth and weaken the spin fluctuations, and then restore a Fermi-liquid ground state with lower  $T_c$ .

Keywords: Fe-based superconductor, pressure effect, non Fermi liquid

(Some figures may appear in colour only in the online journal)

## Introduction

Recently, the hybrid Fe-based superconductors with double FeAs layers have drawn considerable attention as a new platform for rational design of new superconductors and for the exploration of emergent phenomena [1–6]. At present, two well-explored families of hybrid Fe-based superconductors are the ‘1144’-type  $M\text{AeFe}_4\text{As}_4$  and ‘12442’-type  $M(\text{Ae}/R)_2\text{Fe}_4\text{As}_4(\text{F/O})_2$ , in which  $M$  = alkaline metal,

$\text{Ae}$  = alkaline earth metal,  $R$  = rare earth metal. They are obtained through an intergrowth between  $\text{ThCr}_2\text{Si}_2$ -type (122) and/or  $\text{ZrCuSiAs}$ -type (1111) parent compounds of Fe-based superconductors [1, 2, 7, 8]. Because the 122-type  $M\text{Fe}_2\text{As}_2$  such as  $\text{KFe}_2\text{As}_2$  is heavily hole doped [9], both families of hybrid materials are hole doped by itself, making them stoichiometric superconductors without extra carrier doping [2, 5, 7, 10]. At ambient pressure, these double-layer FeAs-hybrid superconductors exhibit a high superconducting transition

at  $T_c \approx 28\text{--}37\text{ K}$ . In addition, the unique asymmetric double  $\text{Fe}_2\text{As}_2$  layer together with the additional structural parameters such as the bilayer thickness (i.e.  $ca$  ratio) make them more complicated than other conventional FeAs-based superconductors [2, 5]. Nonetheless, the lattice/magnetism instabilities, the multi-bands effect, and the spin fluctuations should correlate intimately with the observed unconventional superconductivity [11–14]. Moreover, the Eu-based hybrid superconductors show the robust coexistence of Eu-spin ferromagnetism and superconductivity, providing an ideal platform for further investigations on the correlation between crystal structure, ferromagnetism and superconductivity [3, 15, 16].

$\text{KCa}_2\text{Fe}_4\text{As}_4\text{F}_2$  is a prototype of the ‘12442’ hybrid superconductor with  $T_c = 33.2\text{ K}$ ; it is obtained via an intergrowth between  $\text{KFe}_2\text{As}_2$  and  $\text{CaFeAsF}$  [2]. Following the similar strategy, Cao and co-workers expanded the ‘12442’-type hybrid superconducting family to  $\text{MR}_2\text{Fe}_4\text{As}_4\text{O}_2$  by replacing  $\text{Ca}^{2+}$  with  $\text{R}^{3+}$  and  $\text{F}^-$  with  $\text{O}^{2-}$ , which show superconductivity at  $T_c \approx 33\text{--}37\text{ K}$  due to the intrinsic self-hole doping [5]. In these oxyarsenides, the lattice match between the 1111- and 122-type blocks plays the crucial role for stabilizing the hybrid structure, and the lattice parameters and the bilayer thickness have direct correlations with  $T_c$  [5]. Among them,  $\text{RbGd}_2\text{Fe}_4\text{As}_4\text{O}_2$  is a member with a relatively high  $T_c$  of 35 K, and the high-quality sample can be prepared [10]. At ambient pressure, its normal-state resistivity  $\rho(T)$  exhibits a nice linear-in- $T$  dependence in a wide temperature range of  $T_c < T < 75\text{ K}$ , which is a hallmark of non-Fermi-liquid behavior presumably due to the presence of strong critical spin fluctuations. Similar behavior has been observed in the  $\text{BaFe}_2(\text{As}_{1-x}\text{P}_x)_2$  system [17–20]. Indeed, a very recent Mössbauer spectroscopy study on  $\text{RbGd}_2\text{Fe}_4\text{As}_4\text{O}_2$  has revealed the absence of static magnetic order and broad spectrum associated with the magnetic fluctuations of both Gd and Fe moments [14]. On the other hand, theoretical calculations indicated that  $\text{RbGd}_2\text{Fe}_4\text{As}_4\text{O}_2$  has the multi-band character and a stripe antiferromagnetic ground state resulting from the Fermi surface nesting [21]. These results suggest that  $\text{RbGd}_2\text{Fe}_4\text{As}_4\text{O}_2$  might be located near a magnetic instability with enhanced critical spin fluctuations. As a matter of fact, the formal hole doping level (0.25 electrons/Fe) in  $\text{RbGd}_2\text{Fe}_4\text{As}_4\text{O}_2$  is very close to that in the optimally doped  $\text{Ba}_{1-x}\text{K}_x\text{Fe}_2\text{As}_2$  with  $x = 0.4\text{--}0.5$  where the antiferromagnetic order just disappears [9, 22].

As an effective and clean knob to tune the crystal and electronic structures, high pressure has been widely employed in studying the Fe-based superconductors by either changing the balance of competing interactions or inducing/enhancing  $T_c$  [23–26]. As for ‘1144’-type hybrid superconductors,  $\text{KCaFe}_4\text{As}_4$  and  $\text{KCa}(\text{Fe}_{1-x}\text{Ni}_x)_4\text{As}_4$ , pressure can induce a half-collapsed-tetragonal phase along with the disappearance of bulk superconductivity, similar to the case of  $\text{CaFe}_2\text{As}_2$  [4, 15]. With the help of high-energy x-ray diffraction (XRD) and density functional theory relativistic calculations, the collapsed tetragonal phase was found to result from the crossing As–As bonding to the Ca layer [4]. Given the strong interplay between lattice instability, spin fluctuations and superconductivity in  $\text{RbGd}_2\text{Fe}_4\text{As}_4\text{O}_2$ , in this work we investigate the effect of pressure on the superconducting  $T_c$

and normal-state behaviors by measuring its resistivity  $\rho(T)$  under various pressures to 14 GPa. We found that the  $T_c$  value is suppressed monotonically to ca. 12.5 K upon increasing pressure to 14 GPa with a slope change of  $T_c(P)$  around 4 GPa. The normal state evolves gradually from a non-Fermi liquid (nFL) at ambient pressure to a Fermi liquid (FL) at  $P \geq 4\text{ GPa}$ . Accompanying with the nFL to FL crossover, the effective mass of charge carriers, reflected by the temperature quadratic coefficient of resistivity, displays a significant reduction as commonly observed in the vicinity of a magnetic quantum critical point (QCP). Our results thus indicate that the stoichiometric  $\text{RbGd}_2\text{Fe}_4\text{As}_4\text{O}_2$  might be located near an ambient-pressure QCP such that the enhanced spin fluctuations drive the high- $T_c$  superconductivity.

## Experimental details

Polycrystalline  $\text{RbGd}_2\text{Fe}_4\text{As}_4\text{O}_2$  samples used in this study was synthesized by a solid-state reaction method as described elsewhere [10]. Temperature dependence of resistivity  $\rho(T)$  under various pressures up to 14 GPa were measured with the standard four-probe configuration in a palm cubic anvil cell (CAC) apparatus. The pressure values inside the CAC were calibrated by observing the characteristic transitions of bismuth (Bi) and lead (Pb) at room temperature [27]. We have also determined the pressures at low temperatures by monitoring the superconducting transition of Pb, and the pressure variation upon cooling is less than 0.4 GPa for most pressure values. Glycerol was employed as the pressure-transmitting medium for the high-pressure measurements. Although the hydrostatic limit of glycerol is limited to  $\sim 1.4\text{ GPa}$  [28], the three-axis compression geometry for CAC together with the sample-in-liquid configuration can ensure an excellent pressure homogeneity, as demonstrated by the sharpness of the characteristic transitions of Bi and Pb. The pressure gradient inside the sample capsule at low temperatures is estimated to be less than 0.2 GPa from the superconducting transition width of Pb. We also measured powder XRD at room temperature under various pressures up to 18 GPa with a symmetric diamond anvil cell (DAC) in a laboratory x-ray diffractometer, Rigaku XtaLAB P200, equipped with  $\text{Mo-K}\alpha$  ( $\lambda = 0.71073\text{ \AA}$ ) radiation. The pressure values were determined by the ruby fluorescence.

## Results and discussions

Figure 1(a) shows the temperature dependence of resistivity  $\rho(T)$  in the whole temperature range under various pressures up to 14 GPa. As can be seen,  $\rho(T)$  at ambient pressure exhibits a broad hump centered around  $T^* \sim 170\text{ K}$ , and follows nicely a linear temperature dependence from 100 K down to  $T_c \approx 35\text{ K}$ . All these features are consistent with the previous report [10]. With increasing pressure, the magnitude of  $\rho(T)$  decreases gradually and the broad hump at high temperature fades away quickly, while the superconducting transition decreases monotonically. It has been proposed that the characteristic resistivity hump around  $T^*$  originates from

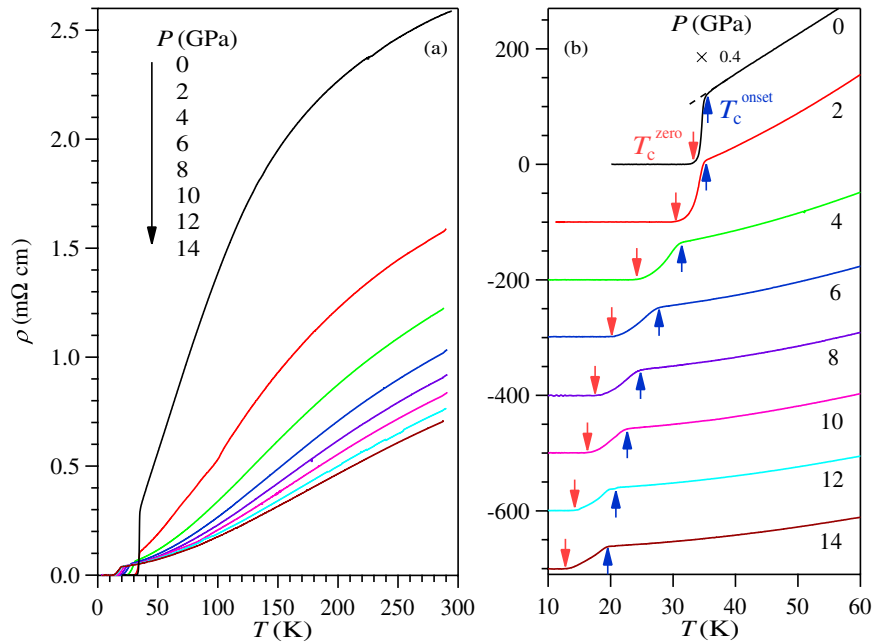


**Figure 1.** High-pressure resistivity for RbGd<sub>2</sub>Fe<sub>4</sub>As<sub>4</sub>O<sub>2</sub>. (a)  $\rho(T)$  curves in the whole temperature range showing the overall resistivity behaviors under various pressures up to 14 GPa. (b)  $\rho(T)$  curves below 60 K showing the variation with pressure of the superconducting transition. The  $\rho(T)$  curve at 0 GPa was scaled by a factor of 0.4. Except for the  $\rho(T)$  curve at 0 GPa, all other curves in (b) have been vertically shifted for clarity. Note: the kink anomaly around 100 K at 2 GPa in (a) is an artifact associated with a change of temperature sweep rate due to an interrupt of heater during the warming-up process.

an incoherent-to-coherent crossover for the 3d electrons in Fe-based superconductors, which is related to the strength of Hund's rule coupling  $J_H$  [29, 30]. This feature involves the interplay between the weak-coupling itinerant electrons (coherent states) and the strong-coupling local moments (incoherent states), as described by the Kondo lattice physics [31, 32]. Pressure can increase the coherent states at the expense of the incoherent states, making the crossover fade away gradually. In order to see more clearly the variation of  $T_c$  with pressure, the  $\rho(T)$  data below 60 K are vertically shifted and displayed in figure 1(b). Here, we define  $T_c^{\text{onset}}$  (up-pointing arrow) as the temperature where  $\rho(T)$  starts to deviate from the extrapolated normal-state behavior, and determine  $T_c^{\text{zero}}$  (down-pointing arrow) as the zero-resistivity temperature. At ambient pressure, the superconducting transition is quite sharp with  $T_c^{\text{onset}} = 35$  K and  $T_c^{\text{zero}} = 34$  K, in excellent agreement with the previous report [10]. With increasing pressure, both  $T_c^{\text{onset}}$  and  $T_c^{\text{zero}}$  decrease continuously and reach  $\sim 20$  K and  $\sim 12.5$  K at 14 GPa.

The pressure dependences of obtained  $T_c^{\text{onset}}$  and  $T_c^{\text{zero}}$  are displayed in figure 2. As can be seen, the transition width  $\Delta T_c (\equiv T_c^{\text{onset}} - T_c^{\text{zero}})$  at  $P > 2$  GPa becomes wider than that at ambient pressure, and keeps at  $\sim 6$ – $8$  K up to the highest pressure. In addition to a negative pressure effect on  $T_c$ , our high-pressure data also reveal a slope change of  $T_c(P)$  at around 4 GPa; e.g.  $T_c^{\text{zero}}$  decreases with pressure in a slope about  $-2.5$  K GPa<sup>-1</sup> for  $0 \leq P \leq 4$  GPa, and  $-1.1$  K GPa<sup>-1</sup> for  $4 < P \leq 14$  GPa. It should be noted that the presence of grain boundaries in the studied polycrystalline sample should not influence the pressure dependence of  $T_c$ . A proper understanding of the pressure effect may help us to understand the superconducting mechanism of the 12442-type

RbGd<sub>2</sub>Fe<sub>4</sub>As<sub>4</sub>O<sub>2</sub>. In this regard, the normal-state properties should provide us important clues. Indeed, a closer inspection of  $\rho(T)$  data in figure 1(b) indicates a clear deviation from the  $T$ -linear behavior upon increasing pressure, which will be discussed in detail below.

Before we analyze the normal-state  $\rho(T)$ , we need to first check if there is any structural transition under pressure. For the 122- and 1144-type FeAs-based superconductors, previous studies have evidenced a collapsed tetragonal phase transition induced by chemical doping or high pressure [33, 34], and the transition can be manifested as a sudden resistivity change [4, 35, 36]. In order to check whether there exists a collapsed tetragonal phase transition in the 12442-type RbGd<sub>2</sub>Fe<sub>4</sub>As<sub>4</sub>O<sub>2</sub>, we replotted in figure 3 the pressure dependence of resistivity data at several fixed temperatures. As can be seen, within the investigated pressure range, the resistivity value at all temperatures decreases smoothly with increasing pressure, implying the absence of collapsed tetragonal phase transition up to 14 GPa for RbGd<sub>2</sub>Fe<sub>4</sub>As<sub>4</sub>O<sub>2</sub>. Since the studied sample is in a polycrystalline form, the reduction of resistivity under pressure may be partially attributed to the improvement of the inter-grain linkage. Nevertheless, the observation of resistivity decreasing in a reduced slope for  $P \geq 4$  GPa at all temperatures is also consistent with the gradually transfer from incoherent to coherent states and the dominance of coherent states under higher pressures [29–32].

Figure 4(a) displays the room-temperature XRD patterns of RbGd<sub>2</sub>Fe<sub>4</sub>As<sub>4</sub>O<sub>2</sub> under various pressures up to 17.73 GPa. No peak splitting or extra diffraction peaks was observed upon compression, thus ruling out the occurrence of any structural phase transition in the measured pressure range, in agreement with the smooth variations of  $\rho(P)$  shown in figure 3. The

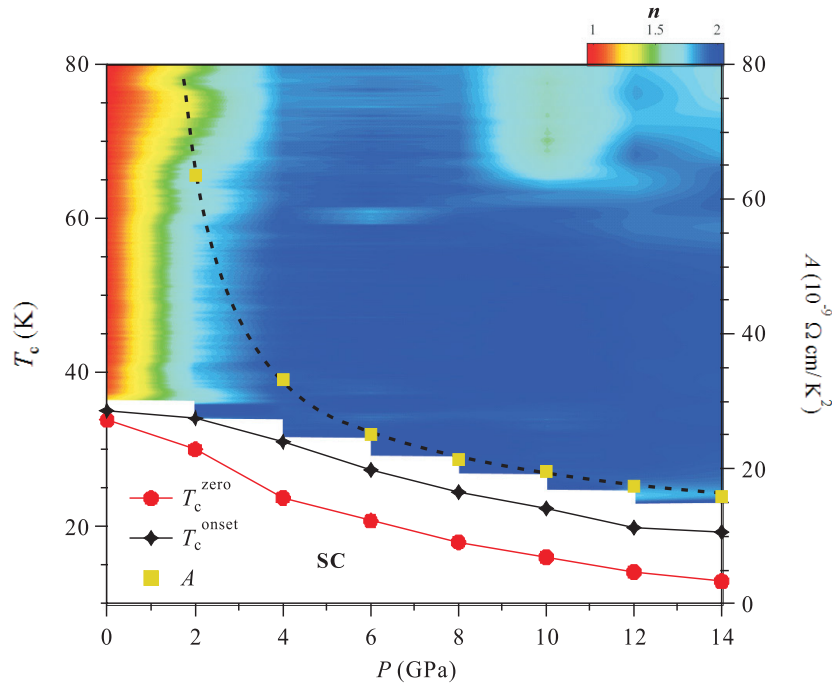


**Figure 2.** Pressure dependence of the superconducting transition temperatures  $T_c^{\text{onset}}$  and  $T_c^{\text{zero}}$  (left), and the quadratic temperature coefficient  $A$  of resistivity (right) for  $\text{RbGd}_2\text{Fe}_4\text{As}_4\text{O}_2$ . The color contour plot shows the temperature exponent  $n$  of resistivity in the normal state up to 14 GPa.

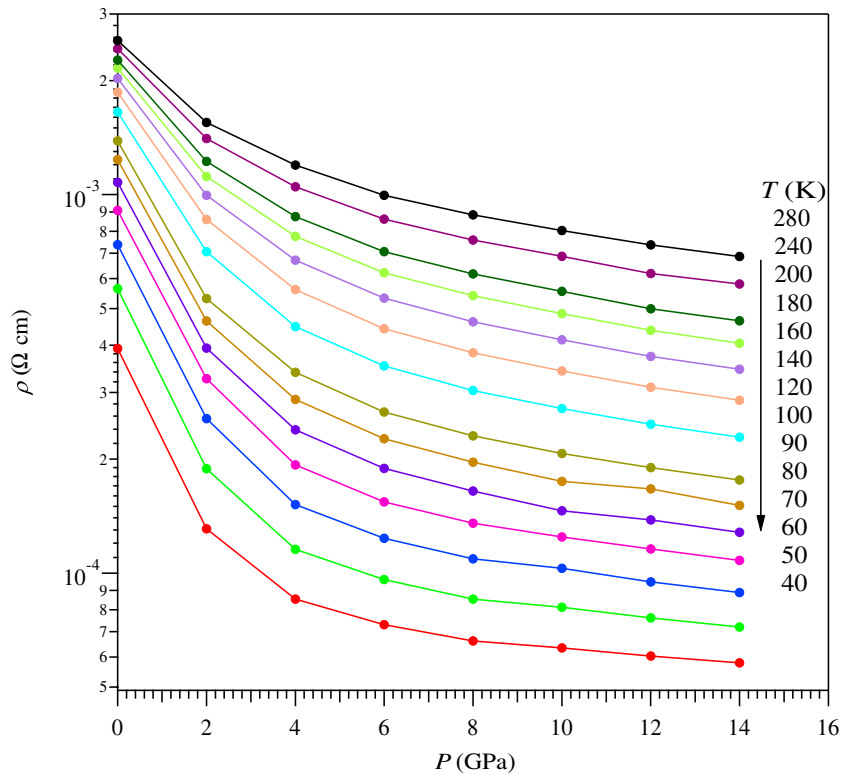


**Figure 3.** Pressure dependence of resistivity  $\rho(P)$  at selected temperatures for  $\text{RbGd}_2\text{Fe}_4\text{As}_4\text{O}_2$ . The resistivity decreases smoothly with pressure without showing any discernible anomaly, implying the absence of collapsed tetragonal phase transition up to 14 GPa.

pressure dependences of lattice parameters  $a$ ,  $c$  and volume  $V$  obtained by the LeBail fit to these XRD patterns in a tetragonal unit cell are displayed in figures 4(b) and (c). As expected for the layered structure, the  $c$  axis is more compressible than the  $a$  axis; i.e. the  $c$  axis is reduced by 9.58% whereas the  $a$

axis shrinks by 3.37% at 17.7 GPa. As a result, the  $c/a$  ratio decreases from 8.06 at ambient pressure to 7.54 at 17.7 GPa. The continuous reduction of  $V(P)$  can be described well with the Birch–Murnaghan equation, which gives the bulk modulus  $B_0 = 71(4)$  GPa, and  $V_0 = 478.7(9) \text{ \AA}^3$ .

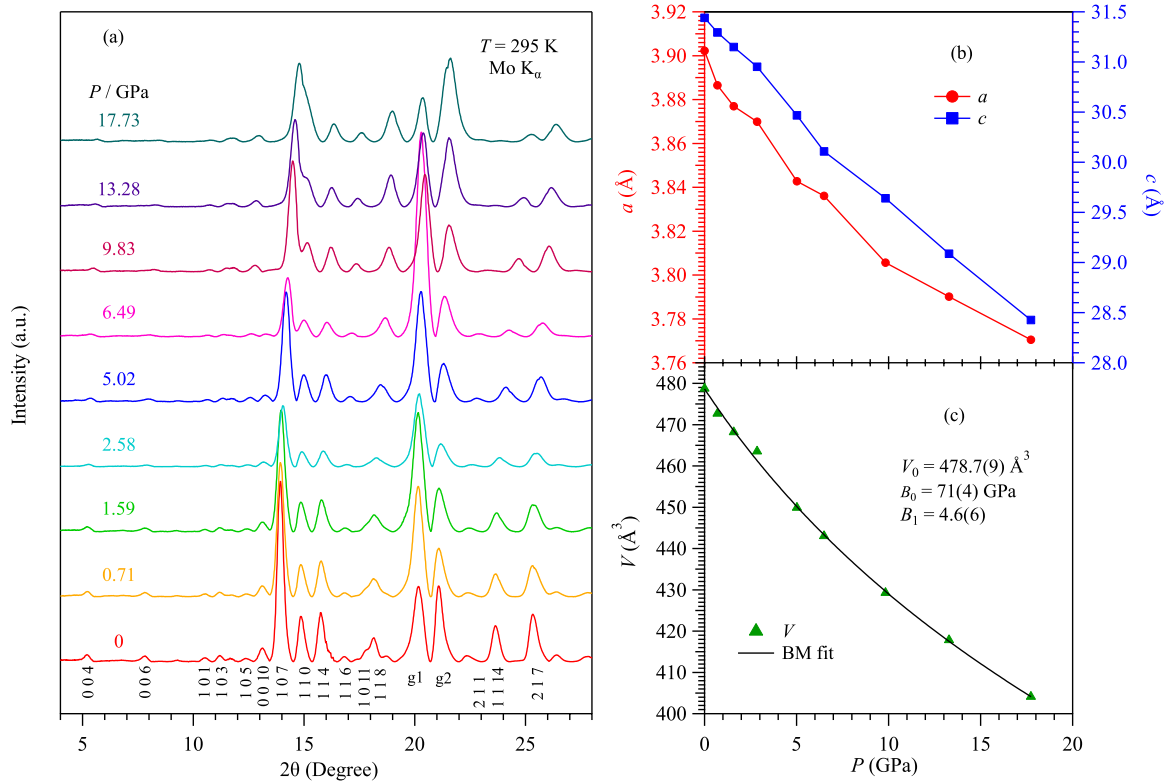


**Figure 4.** (a) Room-temperature XRD patterns of RbGd<sub>2</sub>Fe<sub>4</sub>As<sub>4</sub>O<sub>2</sub> under various pressures up to 17.73 GPa. g1 and g2 denote the diffraction peaks from gasket. (b) and (c) Pressure dependences of lattice parameters  $a$ ,  $c$  and volume  $V$ . The solid line in (c) represents the fit to the Birch–Murnaghan equation.

To gain more insight on the pressure effect on the transport properties, we then analyzed the normal-state  $\rho(T)$  and attempted to establish a connection with the evolution of  $T_c$  under pressure. The  $\rho(T)$  data below 60 K at different pressures are displayed in figures 5(a)–(h), and are fitted with a simple power law  $\rho(T) = \rho_0 + BT^n$ , where  $\rho_0$  is the residual resistivity, and  $n$  is the resistivity exponent. The fitting curves are shown by the broken lines in figure 5, and the results immediately show that the exponent evolves from  $n = 1$  for 0 GPa through  $n = 1.74$  for 2 GPa to  $n \approx 2$  for  $P \geq 4$  GPa. Such an evolution can be visualized more profoundly in a contour plot of the resistivity exponent  $n \equiv \text{dlog}(\rho - \rho_0)/\text{dlog}T$  superimposed in figure 2. These results demonstrate that the nFL state of RbGd<sub>2</sub>Fe<sub>4</sub>As<sub>4</sub>O<sub>2</sub> at ambient pressure is quite fragile and the application of high pressure over 2 GPa can readily restore the FL state, which is reminiscent of the situation commonly seen on the right side of a magnetic QCP [20, 37].

If this is the case, the effective mass of charge carriers will experience a significant reduction as high pressure drives the system away from the QCP. Although the obtained coefficient  $B$  signals such a trend, the variation of exponent  $n$  prevents a quantitative comparison. To this end, we have replotted the  $\rho(T)$  data in the form of  $\rho$  versus  $T^2$  and obtained the quadratic temperature coefficient  $A$  from a linear fitting to the low-temperature region. Since the linear region is quite limited for 0 GPa, we have omitted this pressure, and extract the quadratic temperature coefficients  $A$  for  $P \geq 2$  GPa from the linear fitting to  $\rho(T^2)$  in the low- $T$  region. The pressure dependence of  $A(P)$  is also displayed in figure 2. As can be seen, the coefficient  $A$

decreases quickly upon increasing pressure, and tends to diverge at ambient pressure. Since the coefficient  $A$  is proportional to the carriers effective mass via  $A \propto (m^*/m_0)^2$ , the observed simultaneous reduction of effective mass accompanying with the nFL to FL crossover indicates that RbGd<sub>2</sub>Fe<sub>4</sub>As<sub>4</sub>O<sub>2</sub> might be located in the vicinity of an ambient-pressure magnetic QCP, while the application of high pressure drives the system away from it. It should be noted that the polycrystalline nature of the studied sample might weaken the above quantitative discussions, and more rigorous conclusions can be drawn after single-crystal samples become available.

In the Fe-based superconductors, high- $T_c$  superconductivity usually emerges when the long-range antiferromagnetic order of the parent compound is destabilized by chemical doping or high pressure, resulting in a dome-shaped  $T_c(x, P)$  phase diagram with the optimal  $T_c$  taking place near the antiferromagnetic QCP [23]. In the normal state above QCP, it was commonly found to exhibit prevailing nFL behaviors in a large temperature range and dramatic enhancement of effective mass due to the enhanced critical spin fluctuations [38–40]. These behaviors can be well illustrated in the hole-doped Ba<sub>1-x</sub>K<sub>x</sub>Fe<sub>2</sub>As<sub>2</sub> and chemically pressurized BaFe<sub>2</sub>As<sub>2-x</sub>P<sub>x</sub> [17, 22]. Since the ‘12442’-type RbGd<sub>2</sub>Fe<sub>4</sub>As<sub>4</sub>O<sub>2</sub> is self-hole-doped stoichiometric superconductor with 0.25 holes per Fe, which is close to the optimal doping  $x_c = 0.4$ – $0.5$  in Ba<sub>1-x</sub>K<sub>x</sub>Fe<sub>2</sub>As<sub>2</sub> [22], it is very likely to locate in the vicinity of an ambient-pressure QCP where the antiferromagnetic order just disappears and the superconducting  $T_c$  reaches the maximum. According to the first-principles calculations

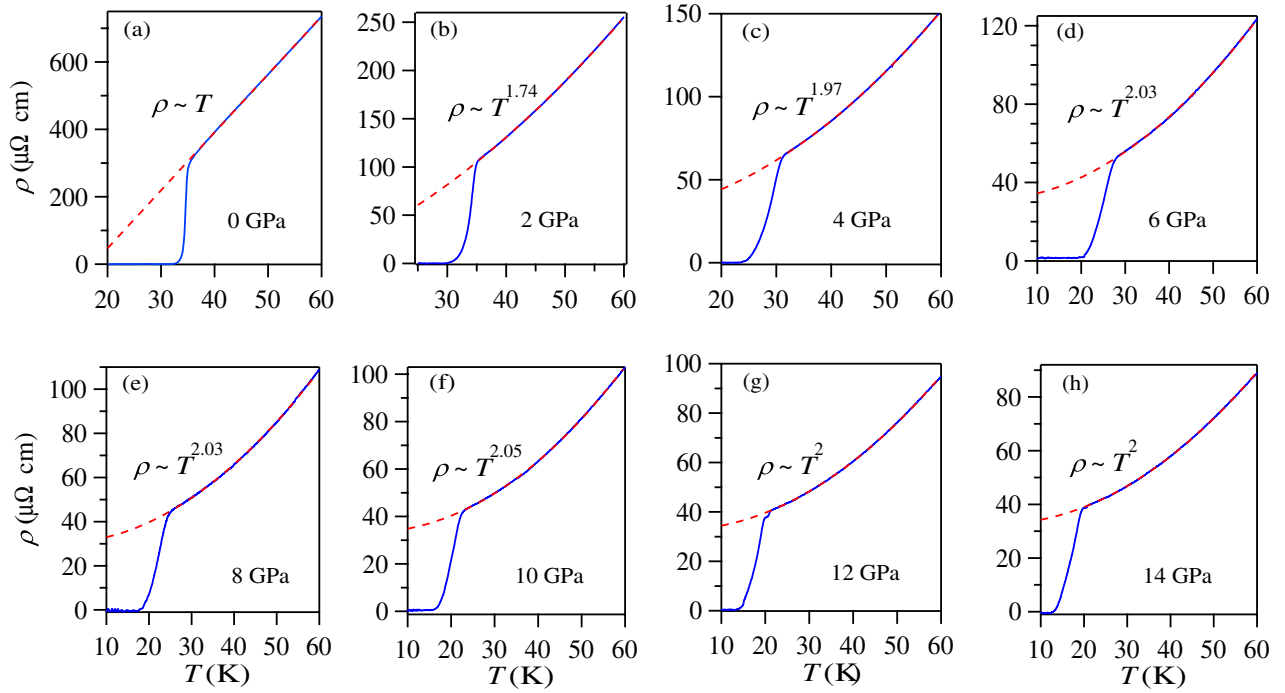


**Figure 5.** Temperature dependence of resistivity  $\rho(T)$  below 60 K under different pressures: (a) 0 GPa, (b) 2 GPa, (c) 4 GPa, (d) 6 GPa, (e) 8 GPa, (f) 10 GPa, (g) 12 GPa, (h) 14 GPa. A simple power law  $\rho(T) = \rho_0 + BT^n$  is applied to fit the normal-state  $\rho(T)$ , as shown by the broken line in each panel.

and Mössbauer spectroscopy study, the ground state of  $\text{RbGd}_2\text{Fe}_4\text{As}_4\text{O}_2$  indeed has strong spin fluctuations as seen in other Fe-based superconductors [21], which can rationalize the observed nFL behavior at ambient pressure. Our present study suggests that the application of high pressure can drive the system away from the QCP and restore the Fermi-liquid state via broadening the electronic bandwidth and weakening the spin fluctuations under pressure.

Finally, it is instructive to compare the results of ‘12442’-type  $\text{RbGd}_2\text{Fe}_4\text{As}_4\text{O}_2$  with those of ‘1144’-type  $\text{CaKFe}_4\text{As}_4$ , which has been well studied recently. For  $\text{CaKFe}_4\text{As}_4$ , inelastic neutron scattering and nuclear magnetic resonance measurements evidenced an enhancement of spin fluctuations below  $T_c$  and supported the  $s_{\pm}$  pairing mechanism [11, 41, 42]. Recent high-pressure studies on  $\text{CaKFe}_4\text{As}_4$  unveiled a half-collapsed tetragonal phase, which is different from the collapsed tetragonal phase of  $\text{CaFe}_2\text{As}_2$  that is non-superconducting in bulk [4]. Upon electron doping in  $\text{CaKFe}_4\text{As}_4$ , i.e. a partial substitution of Co or Ni for Fe, the superconducting phase is gradually suppressed and an antiferromagnetic order can be induced again as observed in resistivity, specific heat, Mössbauer, and neutron diffraction studies [43, 44]. For ‘12442’-type  $(\text{K/Cs})\text{Ca}_2\text{Fe}_4\text{As}_4\text{F}_2$ , muon spin rotation ( $\mu\text{SR}$ ) measurements indicated that they exhibit multiple-gap superconductivity with an  $s + d$  gap symmetry [12, 45]. Similarly, the first-principles calculations and Mössbauer measurements also evidenced a multi-band character and enhanced spin fluctuations in the  $\text{RbGd}_2\text{Fe}_4\text{As}_4\text{O}_2$  [21]. In contrast, our high-pressure resistivity and XRD data in figures 3 and 4 indicated the absence of half-collapsed tetragonal phase transition in  $\text{RbGd}_2\text{Fe}_4\text{As}_4\text{O}_2$  at least up to 18 GPa.

## Conclusions

In summary, we have performed high-pressure resistivity measurements on the newly synthesized ‘12442’-type  $\text{RbGd}_2\text{Fe}_4\text{As}_4\text{O}_2$ , which is a self-hole-doped stoichiometric hybrid superconductor with double FeAs layers. We found that pressure can suppress  $T_c$  progressively from 35 K at 0 GPa to  $\sim 12.5$  K at 14 GPa with a slope change of  $T_c(P)$  at around 4 GPa. Pressure dependent of resistivity at fixed temperatures and high-pressure XRD at room temperature rule out the occurrence of half-collapsed tetragonal phase transition up to 18 GPa. In addition, the normal state  $\rho(T)$  was found to evolve gradually from nFL for  $P < 4$  GPa to FL at  $P \geq 4$  GPa accompanied by a significant reduction of effective mass. These results thus indicate that the stoichiometric  $\text{RbGd}_2\text{Fe}_4\text{As}_4\text{O}_2$  might be located near an ambient-pressure QCP. The enhanced critical spin fluctuations should play an important role for mediating high- $T_c$  superconductivity at ambient pressure, while the application of high pressure drives the system away from the QCP and restores the Fermi-liquid ground state with lower  $T_c$ .

## Acknowledgments

This work is supported by the National Natural Science Foundation of China (grant nos. 11574377, 11834016, 11874400), the National Key R&D Program of China (grant nos. 2018YFA0305702 and 2018YFA0305800), the Strategic Priority Research Program and Key Research Program of Frontier Sciences of the Chinese Academy of Sciences (grant nos. XDB25000000 and QYZDB-SSW-SLH013). JPS

acknowledges support from the Postdoctoral Innovative Talent program and China Postdoctoral Science Foundation.

## ORCID iDs

J-G Cheng  <https://orcid.org/0000-0002-4969-1960>

## References

- [1] Iyo A *et al* 2016 *J. Am. Chem. Soc.* **138** 3410
- [2] Wang Z C, He C Y, Wu S Q, Tang Z T, Liu Y, Ablimit A, Feng C M and Cao G H 2016 *J. Am. Chem. Soc.* **138** 7856
- [3] Liu Y *et al* 2016 *Phys. Rev. B* **93** 214503
- [4] Kaluarachchi U S *et al* 2017 *Phys. Rev. B* **96** 140501
- [5] Wu S Q, Wang Z C, He C Y, Tang Z T, Liu Y and Cao G H 2017 *Phys. Rev. Mater.* **1** 044804
- [6] Wang Z-C, He C-Y, Wu S-Q, Tang Z-T, Liu Y and Cao G-H 2017 *Chem. Mater.* **29** 1805
- [7] Iyo A, Kawashima K, Ishida S, Fujihisa H, Gotoh Y, Eisaki H and Yoshida Y 2018 *J. Phys. Chem. Lett.* **9** 868
- [8] Bao J K, Willa K, Smylie M P, Chen H J, Welp U, Chung D Y and Kanatzidis M G 2018 *Cryst. Growth Des.* **18** 3517
- [9] Rotter M, Tegel M and Johrendt D 2008 *Phys. Rev. Lett.* **101** 107006
- [10] Wang Z C *et al* 2017 *J. Phys.: Condens. Matter* **29** 11LT01
- [11] Cho K *et al* 2017 *Phys. Rev. B* **95** 100502
- [12] Kirschner F K K, Adroja D T, Wang Z C, Lang F, Smidman M, Baker P J, Cao G H and Blundell S J 2018 *Phys. Rev. B* **97** 060506
- [13] Fente A, Meier W R, Kong T, Kogan V G, Bud'ko S L, Canfield P C, Guillaumon I and Suderow H 2018 *Phys. Rev. B* **97** 134501
- [14] Li Y *et al* 2018 *Physica C* **548** 21
- [15] Jackson D E *et al* 2018 *Phys. Rev. B* **98** 014518
- [16] Smylie M P *et al* 2018 *Phys. Rev. B* **98** 104503
- [17] Shibauchi T, Carrington A and Matsuda Y 2014 *Annu. Rev. Condens. Matter Phys.* **5** 113
- [18] Nakai Y *et al* 2010 *Phys. Rev. Lett.* **105** 107003
- [19] Walmsley P *et al* 2013 *Phys. Rev. Lett.* **110** 257002
- [20] Kasahara S *et al* 2010 *Phys. Rev. B* **81** 184519
- [21] Wang Z W, Wang G T and Tian X 2017 *J. Alloys Compd.* **708** 392
- [22] Chen H *et al* 2009 *Europhys. Lett.* **85** 17006
- [23] Stewart G R 2011 *Rev. Mod. Phys.* **83** 1589
- [24] Sun J P *et al* 2016 *Nat. Commun.* **7** 12146
- [25] Athena S S 2011 *Rep. Prog. Phys.* **74** 124502
- [26] Luo X G and Chen X H 2015 *Sci. China Mater.* **58** 77
- [27] Cheng J G, Matsubayashi K, Nagasaki S, Hisada A, Hirayama T, Hedo M, Kagi H and Uwatoko Y 2014 *Rev. Sci. Instrum.* **85** 093907
- [28] Angel R J, Bujak M, Zhao J, Gattac G D and Jacobsen S D 2007 *J. Appl. Cryst.* **40** 26–32
- [29] Iimura S, Matsuishi S and Hosono H 2016 *Phys. Rev. B* **94** 024512
- [30] Haule K and Kotliar G 2009 *New J. Phys.* **11** 025021
- [31] Wu Y P, Zhao D, Wang A F, Wang N Z, Xiang Z J, Luo X G, Wu T and Chen X H 2016 *Phys. Rev. Lett.* **116** 147001
- [32] Hardy F *et al* 2013 *Phys. Rev. Lett.* **111** 027002
- [33] Yu W, Aczel A A, Williams T J, Bud'ko S L, Ni N, Canfield P C and Luke G M 2009 *Phys. Rev. B* **79** 020511
- [34] Saha S R, Butch N P, Drye T, Magill J, Ziemak S, Kirshenbaum K, Zavalij P Y, Lynn J W and Paglione J 2012 *Phys. Rev. B* **85** 024525
- [35] Nakajima Y, Wang R X, Metz T, Wang X F, Wang L M, Cynn H, Weir S T, Jeffries J R and Paglione J 2015 *Phys. Rev. B* **91** 060508
- [36] Wang B S *et al* 2016 *Phys. Rev. B* **94** 020502
- [37] Cheng J G, Matsubayashi K, Wu W, Sun J P, Lin F K, Luo J L and Uwatoko Y 2015 *Phys. Rev. Lett.* **114** 117001
- [38] Moriya T and Ueda K 2000 *Adv. Phys.* **49** 555
- [39] Taillefer L 2010 *Annu. Rev. Condens. Matter Phys.* **1** 51
- [40] Sachdev S and Keimer B 2011 *Phys. Today* **64** 29
- [41] Xie T *et al* 2018 *Phys. Rev. Lett.* **120** 267003
- [42] Ding Q P, Meier W R, Bohmer A E, Budko S L, Canfield P C and Frukawa Y 2017 *Phys. Rev. B* **96** 220510
- [43] Kreyssig A *et al* 2018 *Phys. Rev. B* **97** 224521
- [44] Meier W R *et al* 2018 *NPJ Quantum Mater.* **3** 5
- [45] Smidman M, Kirschner F K K, Adroja D T, Hillier A D, Lang F, Wang Z C, Cao G H and Blundell S J 2018 *Phys. Rev. B* **97** 060509